

# Universal power-law scaling in the packing structure of frictional granular materials

Jiajun Tang,<sup>1</sup> Xiaohui Wen<sup>⊗</sup>,<sup>1</sup> Zhen Zhang<sup>⊗</sup>,<sup>1,\*</sup> and Yujie Wang<sup>1,2,3,†</sup>

<sup>1</sup>*Department of Physics, Chengdu University of Technology, Chengdu 610059, China*

<sup>2</sup>*State Key Laboratory of Geohazard Prevention and Geoenvironment Protection, Chengdu University of Technology, Chengdu 610059, China*

<sup>3</sup>*School of Physics and Astronomy, Shanghai Jiao Tong University, Shanghai 200240, China*



(Received 5 September 2024; accepted 3 January 2025; published 15 January 2025)

Friction-induced energy dissipation is one of the key factors contributing to the unique properties of granular materials, such as the preparation history dependence of the packing structure. However, it remains unclear whether or not more realistic systems that involve two or more types of friction possess unique properties distinct from those that are frictionless or with a single type of friction. Here, we use numerical simulations to investigate the packing structure of binary mixtures of particles with particle type-dependent friction coefficient. Taking single-component systems as reference, we use an effective friction coefficient  $\mu_e$  to represent the overall frictional strength in granular systems prepared via different protocols. Our results demonstrate that  $\mu_e$  exhibits a power-law dependence on the individual friction coefficients. Furthermore, we propose models that accurately predict the packing structure of frictional particle systems across a range of compositions, size ratios, and preparation protocols.

DOI: [10.1103/PhysRevE.111.015420](https://doi.org/10.1103/PhysRevE.111.015420)

## I. INTRODUCTION

Granular materials such as sands and powders are ubiquitous in many industrial processes and geophysical phenomena [1–5]. These systems are intrinsically in nonequilibrium due to their athermal nature and complex energy dissipation processes [3,6–8]. When subjected to external drives, granular systems evolve into stationary packings.

Interparticle friction plays a crucial role in determining the packing structure by affecting the mechanical stability of the system [3,9–15]. Specifically, increased friction can expand the packing fraction range of granular packings, which varies from random loose packing to random close packing [14,16–18]. Previous studies have shown that the loosest packing structure that forms under a given condition depends strongly on friction [19–22], as friction increases the density of states for mechanically stable configurations [23,24]. Friction complicates the stress network within the system, leading to varied responses of the system to external drives, which in turn results in different packing structures [11,23,25–29]. Despite the importance of friction in granular packing, understanding their relationship has been challenging since it might also depend on the preparation history of the packing structure [5].

So far, studies have mainly been focused on granular systems that involve only a single type of friction, ignoring the complexities arising from the coexistence of two or more types of friction coefficients. However, in both natural and industrial settings, granular systems are usually composed of particles with distinct frictional characteristics, which can have a significant influence on the flowability, packing effi-

ciency, and mechanical stability of these materials [30–36]. Understanding the effects of multiple coexisting friction coefficients on the packing structure and properties of granular systems is thus of both fundamental and practical importance.

In this work, we are motivated to understand the influence of friction, focusing on how individual friction coefficients are coupled to influence the packing structure. By analyzing the differences in particle packing structures, we study the macroscopic friction effects in binary mixtures with frictional particles. We find that the packing fractions of different systems collapse onto a master curve that depends solely on friction. Furthermore, we uncover a universal power-law relationship associated with the coupling of multiple friction effects, which allows us to simplify the influence of friction in multicomponent systems to that of a single-component system. These findings are useful for understanding the impact of friction on the performance of granular materials in complex scenarios.

## II. MODEL AND METHOD

Molecular dynamics (MD) simulations were performed for both single- and two-component frictional particle systems using the Large-scale Atomic/Molecular Massively Parallel Simulator (LAMMPS) software [37]. The interactions between the particles were described by the Hertz-Mindlin no-slip model, which has previously been successfully used to study the properties of particle systems [38–40]. The normal component  $\mathbf{F}_{ij}^{(n)}$  and tangential component  $\mathbf{F}_{ij}^{(t)}$  of the contact force between particles  $i$  and  $j$  were given by

$$\mathbf{F}_{ij}^{(n)} = \frac{4}{3} E_{ij} (R_{ij})^{1/2} \alpha^{3/2} \mathbf{n}_{ij} - \beta_n \mathbf{v}_{ij}^{(n)}, \quad (1)$$

$$\mathbf{F}_{ij}^{(t)} = -k_t \alpha \delta \mathbf{t}_{ij} - \beta_t \mathbf{v}_{ij}^{(t)}. \quad (2)$$

\*Contact author: zhen.zhang@cdut.edu.cn

†Contact author: yujiewang@sjtu.edu.cn

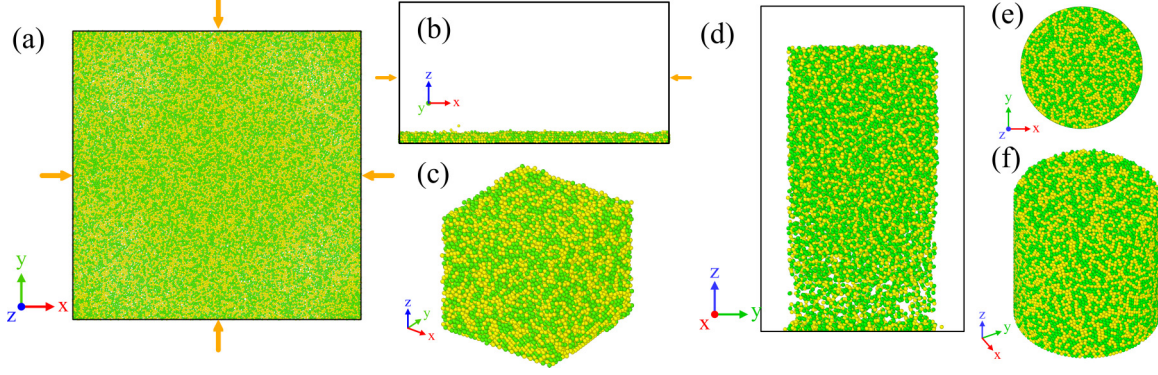


FIG. 1. (a)–(c) Schematic illustration of the simulation process for preparing the packing structure using biaxial compression. (d)–(e) Schematic illustration of the protocol to prepare the packing structure through random pouring. A and B particles are represented as balls in red and blue, respectively.

For the normal force  $\mathbf{F}_{ij}^{(n)}$ ,  $E_{ij} = [(1 - v_i^2)E_i^{-1} + (1 - v_j^2)E_j^{-1}]^{-1}$  is the effective Young's modulus, where  $v_i$  and  $E_i$  are respectively the Poisson's ratio and Young's modulus of particle  $i$ ;  $R_{ij} = (R_i^{-1} + R_j^{-1})^{-1}$  is the effective radius, where  $R_i$  the radius of particle  $i$ ;  $\alpha = R_i + R_j - \|\mathbf{r}_{ij}\|$  is the particle's normal overlap, where  $\mathbf{r}_{ij} = \mathbf{r}_i - \mathbf{r}_j$  and  $\mathbf{r}_i$  is the position vector of particle  $i$ ;  $\mathbf{n}_{ij} = \mathbf{r}_{ij}/\|\mathbf{r}_{ij}\|$  is the normal unit vector,  $\beta_n$  the normal damping, and  $\mathbf{v}_{ij}^{(n)} = [(\mathbf{v}_j - \mathbf{v}_i) \cdot \mathbf{n}_{ij}]\mathbf{n}_{ij}$  the normal component of relative velocity, with  $\mathbf{v}_i$  the velocity vector of particle  $i$ . For the tangential force  $\mathbf{F}_{ij}^{(t)}$ ,  $k_t = 8G_{ij}$ , where  $G_{ij} = [(1 - v_i^2)G_i^{-1} + (1 - v_j^2)G_j^{-1}]^{-1}$  is the effective shear modulus with  $G_i$  the shear modulus of particle  $i$ ;  $a = \sqrt{R_{ij}\alpha}$  is the radius of the contact region, which is perpendicular to the line connecting the centers of the two particles when they are in contact;  $\delta$  is the integrated tangential displacement, which accounts for sliding and rolling motion;  $\beta_t$  is tangential damping;  $\mathbf{v}_{ij}^{(t)} = \mathbf{v}_j - \mathbf{v}_i - \mathbf{v}_{ij}^{(n)} - (R_i\boldsymbol{\omega}_i + R_j\boldsymbol{\omega}_j) \times \mathbf{n}$  is the relative tangential velocity at the point of contact with  $\boldsymbol{\omega}_i$ , the angular velocity vector of particle  $i$ ;  $\mathbf{t}_{ij} = \mathbf{v}_{ij}^{(t)}/\|\mathbf{v}_{ij}^{(t)}\|$  is the tangential unit vector. Static friction was implemented by truncating the tangential force  $\mathbf{F}_{ij}^{(t)}$  to satisfy the Coulomb yield criteria  $\|\mathbf{F}_{ij}^{(t)}\| < \|\mu\mathbf{F}_{ij}^{(n)}\|$ , where  $\mu$  is the static friction coefficient.

In this system, particles of types A and B have diameters of  $d_A$  and  $d_B$ , respectively.  $\mu_A$  and  $\mu_B$  are the interparticle friction coefficients between two A particles and two B particles, respectively. For the friction between type A and type B particles ( $\mu_{AB}$ ), we considered it to be the geometric mean ( $\mu_{AB} = \sqrt{\mu_A\mu_B}$ ) or arithmetic mean ( $\mu_{AB} = (\mu_A + \mu_B)/2$ ). We found that the main conclusions of this work are basically independent of the specific choice of  $\mu_{AB}$  (see next section).

We used two protocols to prepare the packing structure, namely compression and random deposition. Our simulations considered the following values for both  $\mu_A$  and  $\mu_B$ : 0.01, 0.1, 0.2, 0.3, 0.4, 0.5, 0.6, 0.7, 0.8, 0.9, and 1.0. In the compression protocol, particles were first randomly generated in a simulation box of dimensions  $140d \times 140d \times 50d$  ( $x \times y \times z$ ), where  $d$  is the diameter of the A particle. Under gravity, the particles settled to the bottom of the simulation box, forming a loose two-dimensional structure, as shown in Fig. 1(a). Compression of the box was achieved by reducing its dimensions along the  $x$  and  $y$  axes at a constant compressive

strain rate of  $0.0025 \tau^{-1}$  ( $\tau$  is the time unit) while keeping the dimension along the  $z$ -axis constant, as illustrated in Fig. 1(b). The compression terminated when the  $x$  and  $y$  dimensions were reduced to  $30d$ . Fig. 1(c) shows the representative final structure after compression. In this protocol, we considered only the case where particles  $d_A = d_B$ , since a size-dispersed system under compression would result in phase separation. To study the compositional effect, we performed simulations for  $x = 0.5$  and  $x = 0.8$ , where  $x$  is the number fraction of A particles. We performed 800 000 simulation steps under the NVE ensemble, with a time step of  $0.001\tau$ . This included 100 000 steps for generating the particles, 600 000 steps for compression, and 100 000 steps to allow the packing structure to become stable.

In the random deposition protocol, we first generated particles in a cylindrical space and then allowed these particles to fall into a cylindrical container under gravity to obtain a three-dimensional packing structure, as shown in Figs. 1(d)–1(f). The size of the simulation box was  $50d \times 50d \times 80d$  ( $x \times y \times z$ ), and the diameter and height of the cylindrical container were  $40d$ . Since the total volume of the final structure was fixed, the number of particles in the container ranged from about 20 000 to 60 000, depending on composition. We introduced size dispersity by setting  $d_B = \alpha d_A$  [41], where  $\alpha = 1.0, 1.2, \text{ and } 1.4$ . For  $\alpha = 1.2$  and  $1.4$ , we considered three compositions  $x = 0.2, 0.5, \text{ and } 0.8$ . We performed 100 000 simulation steps under the NVE ensemble, with a time step of  $0.001\tau$ . This included the time for generating the particles and stabilizing the packing structure.

### III. RESULTS AND DISCUSSION

Figure 2 shows the packing fraction  $\phi$  and coordination number  $z$  as a function of friction coefficient  $\mu$  for the one-component system. First, we note that both  $\phi$  and  $z$  decrease with the increase of  $\mu$ , compatible with the results of Slibert [14] (also included in the graph). The small difference between the two results over the same range of  $\mu$  might be attributed to the influence of gravity, which was considered in our simulations while not accounted for in the work of Slibert. Since gravity can cause particle overlap to a certain degree, it is reasonable to observe an increase in the values of  $\phi$  and  $z$ .

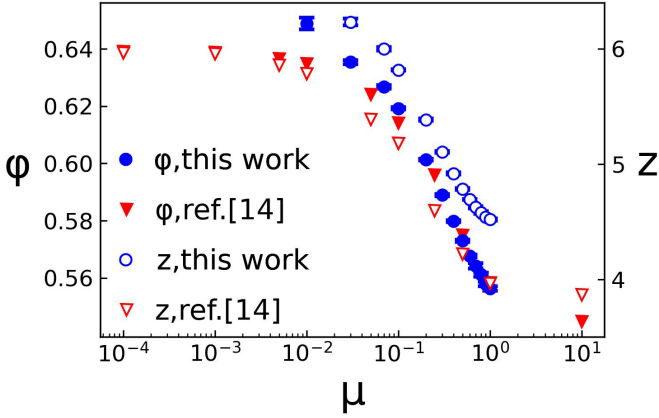
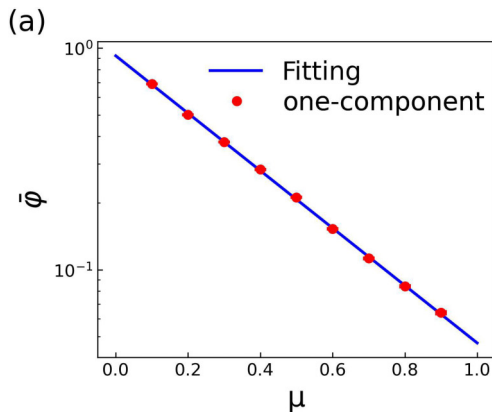


FIG. 2. Packing fraction  $\phi$  and coordination number  $z$  as a function of friction coefficient  $\mu$  in a monodisperse system. The blue circles represent our results, while the red triangles are data extracted from Slibert [14]. Solid symbols denote packing fractions, whereas empty symbols represent coordination numbers.

Furthermore, given that the packing fraction  $\phi$  typically varies with the protocol used to prepare the granular structure, we first unify the range of variation of the packing fraction by defining the normalized packing fraction  $\bar{\phi} = (\phi - k\phi_{\min})/(\phi_{\max} - k\phi_{\min})$ , where  $\phi_{\max}$  and  $\phi_{\min}$  denote the maximum and minimum values of the packing fraction, respectively. We introduce a scaling factor  $k = 0.99$  to ensure that  $\bar{\phi} \neq 0$  when friction  $\mu = 1$ . This scaling allows us to better observe the relationship between  $\bar{\phi}$  and friction on a logarithmic scale. Importantly, this scaling primarily affects the data presentation on a logarithmic scale without altering the underlying relationships between  $\bar{\phi}$  and  $\mu$ . Specifically, the expected value of effective friction  $\mu_e$ , as shown in Fig. 3(b), remains unaffected by this scaling.

Figure 3(a) shows the  $\bar{\phi}$  as a function of the friction coefficient  $\mu$  in the single-component system prepared by the compression method. One observes that  $\bar{\phi}$  depends exponentially on  $\mu$ , that is,

$$\bar{\phi}(\mu) = P_0 \exp(P_1 \mu), \quad (3)$$



where  $P_0 = 0.924$  and  $P_1 = -2.984$  are the fitting parameters that depend on the preparation protocol of the packing structure. Analogous to single-component systems, we define an effective friction  $\mu_e$  to measure the macroscopic friction effect in binary systems. Specifically, the  $\mu_e$  for a binary mixture is equal to the friction coefficient of a single-component system with the same packing fraction for the same preparation protocol. We note that the “effective friction” defined here and used throughout the paper is different from the usages of this term in other fields, for example, for denoting the ratio of shear stress to pressure [42]. This relationship provides a reference for estimating  $\mu_e$  in systems with multiple friction coefficients. For instance, Fig. 3(b) presents the  $\mu_e$  for the  $x = 0.5$  mixture based on the relation as given by Eq. (3) for various values of  $\mu_B$  and  $\mu_A$  (different points with the same symbol type). Overall, one recognizes that the larger the  $\mu_B$ , the smaller the packing fraction, which is consistent with previous findings that stronger friction leads to less efficient packing.

Having determined the effective friction coefficient  $\mu_e$ , we explored its dependence on the individual friction coefficients  $\mu_A$  and  $\mu_B$ , (see Fig. 4, log-log scale). One observes that  $\mu_e$  shows a nice power-law dependence on  $\mu_A$ , that is,  $\mu_e \propto \mu_A^a$ , where  $c$  is a constant and  $a$  is the exponent. Similarly, we find  $\mu_e \propto \mu_B^b$  [see panels (c), (d)]. Therefore, we can further write a general expression:

$$\mu_e \propto \mu_A^a * \mu_B^b. \quad (4)$$

On the condition that  $\mu_e = \mu_A = \mu_B$  if  $\mu_A = \mu_B$ , the three coefficients must satisfy that  $a + b = 1$ . Interestingly, we observe that, for a given composition, for example,  $x = 0.5$ ,  $a = b = 0.5$ , that is, consistent with their respective concentrations. Hence, by assuming that  $a:b = x:(1-x)$ , Eq. (2) can be rewritten as

$$\mu_e = \mu_A^x * \mu_B^{1-x}. \quad (5)$$

To validate Eq. (5), we used it to calculate the potential values of  $\mu_e$  for different systems. Fig. 5(a) shows the calculated  $\mu_e$  versus the normalized packing density. The red and green gradient colors represent compositions  $x = 0.5$  and

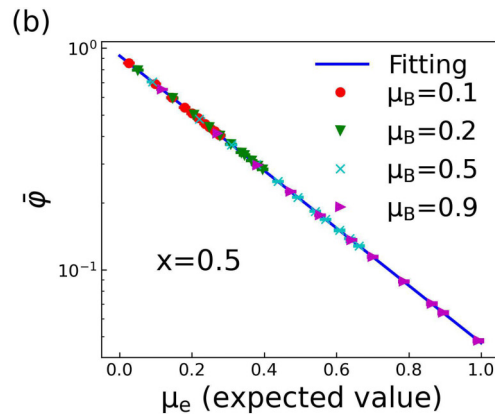


FIG. 3. (a) The normalized packing fraction  $\bar{\phi}$  as a function of the friction coefficient  $\mu$  in the single-component system. The blue curve is an exponential fitting to the data. (b)  $\bar{\phi}$  as a function of the effective packing fraction  $\mu_e$  for the two-component system at various  $\mu_B$ .  $\mu_e$  was obtained by mapping the packing fraction to the fitting line in panel (a).

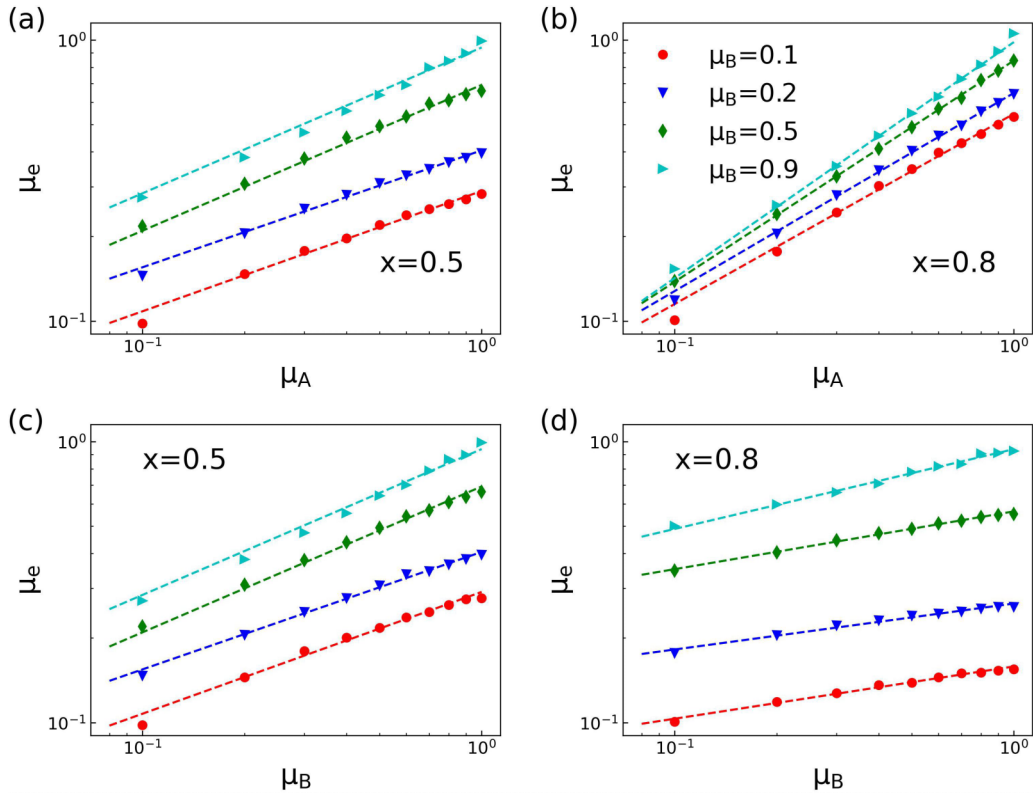


FIG. 4. The effective friction coefficient  $\mu_e$  as a function of the individual friction coefficient  $\mu_\alpha$ . The dashed lines are fits to the various datasets.

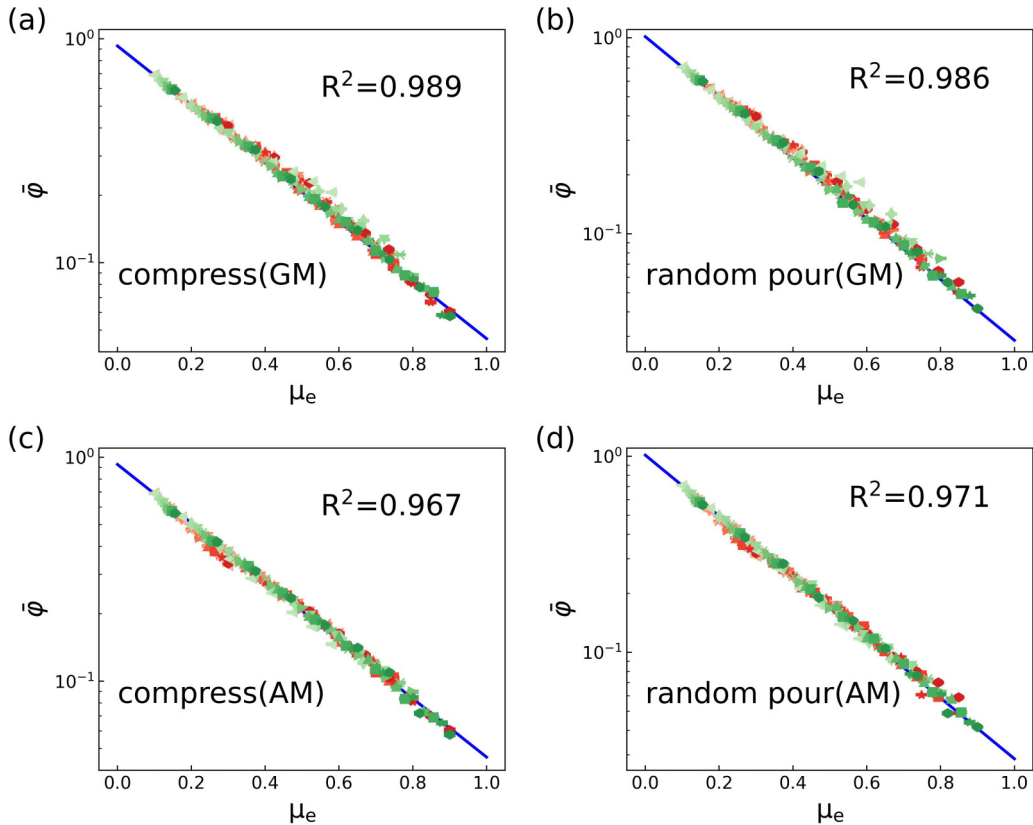


FIG. 5. Correlation between the normalized packing fraction  $\bar{\phi}$  and effective friction coefficient  $\mu_e$  under two preparation methods. (a)–(b)  $\mu_{AB} = \sqrt{\mu_A \mu_B}$ . (c), (d)  $\mu_{AB} = (\mu_A + \mu_B)/2$ . The blue solid line is an exponential fit as shown in Fig. 3(a). The reddish and greenish colors represent the compositions  $x = 0.5$  and  $x = 0.8$ , respectively. The change of color from light to dark corresponds to an increase in  $\mu_B$ .

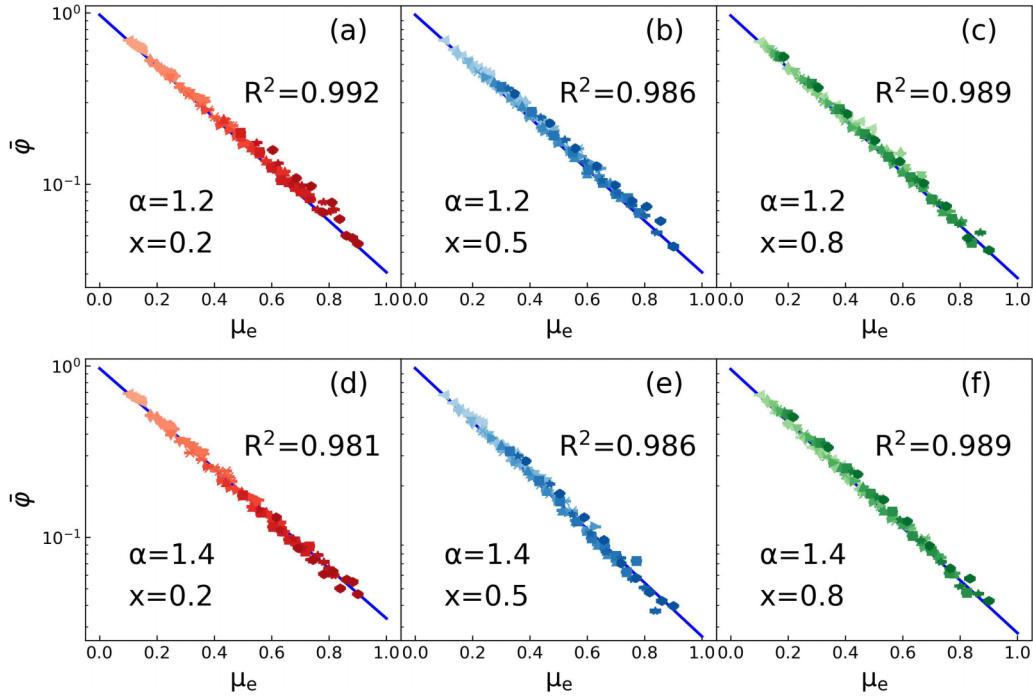


FIG. 6. Correlation between the normalized packing fraction  $\bar{\varphi}$  and effective friction coefficient  $\mu_e$  for  $\alpha = 1.2$  (a)–(c) and  $\alpha = 1.4$  (d)–(f). The change of color from light to dark corresponds to an increase in  $\mu_B$ .

$x = 0.8$ , respectively. We find that these data points are well distributed around the reference line, which is determined from a single-component system, as shown in Fig. 3(a). This alignment confirms that Eq. (5) accurately captures the effective friction in multicomponent systems. Furthermore, we tested the universality of Eq. (5) by applying it to binary systems prepared using a random-pour method. We find that the calculated results also align well with the reference line, as shown in Fig. 5(b), demonstrating the robustness of our functional form across different preparation protocols.

Figures 5(c)–5(d) show the correlation between the normalized packing fraction and  $\mu_e$  for  $\mu_{AB} = (\mu_A + \mu_B)/2$ . The results are nearly identical to those obtained for  $\mu_{AB} = \sqrt{\mu_A \mu_B}$ , panels (a), (b), demonstrating that the macroscopic frictional effects observed in the binary system are independent of the specific definition of  $\mu_{AB}$ .

We use residual analysis to evaluate the goodness of fit between the data points and Eq. (5). Specifically, we use the coefficient of determination  $R^2 = 1 - \text{SSR}/\text{SST}$ , where  $R^2$  varies from 0 to 1 and a larger  $R^2$  indicates a better fit. Here, SSR represents the sum of the squares of the differences between the predicted and actual values, while SST represents the sum of the squares of the differences between the actual and mean values. Based on  $R^2$ , one concludes that Eq. (5) provides an accurate description of the data distribution.

The essence of Eq. (5) lies in the geometric mean of friction across all particles, which is closely related to the nonlinear relationship between packing density and friction. Frictional granular systems can remain stable at densities above their critical density. Consequently, the stability of a mixture of particles with different friction coefficients is primarily determined by the low-friction particles, as they require a higher packing density to maintain stability. Geometric averaging,

which is equivalent to arithmetic mean on a logarithmic scale, better captures the significant impact of small-friction particles.

So far, our analysis has focused on systems with uniform particle sizes. To extend the applicability of Eq. (4) to systems with particle size disparities, we introduce the size ratio  $\alpha = d_B/d_A$ . In binary mixtures of particles with different sizes, the contact modes between different types of particles differ significantly from those in a system with  $\alpha = 1$ . These different contact modes have a significant impact on the forces between particles and the contact area, which Eq. (5) does not explicitly account for. Therefore, directly using it to calculate  $\mu_e$  may not yield ideal results.

Due to the frictional effects existing only between particle contacts, we scale the coefficients  $a$  and  $b$  in Eq. (4) to account for the influence of particle size differences on the overall particle arrangement. Structural analysis at both local and extended levels reveals that larger particles play a more significant role in determining the average structural properties of the system. Consequently, larger particles should contribute more to the macroscopic friction effects. This influence is also composition dependent, leading us to introduce the mean particle diameter  $\bar{d} = x d_A + (1 - x) d_B$  to capture the interaction between concentration and particle size differences. Based on this, we set the coefficients  $a:b = x(d_A)^3 : (1 - x)(d_B/\bar{d})^3$ , with  $\bar{d}$  appearing only in the coefficient for the B particles, indicating the dominant role of the larger particles. The cubic power arises from the effect of the particle size ratio on the average packing fraction [43]. Therefore,  $\mu_e$  can be written as

$$\mu_e = \mu_A^{\frac{x}{x+(1-x)(\alpha/\bar{d})^3}} * \mu_B^{\frac{(1-x)(\alpha/\bar{d})^3}{x+(1-x)(\alpha/\bar{d})^3}}. \quad (6)$$

In the special case of  $\alpha = 1$  or  $x = 0$  or  $1$ , Eq. (6) recovers to Eq. (5).

Figure 6 shows the results for particle size ratios  $\alpha = 1.2$  and  $\alpha = 1.4$  for the binary mixtures as prepared by random pouring. We observe that data for different concentrations are distributed along the corresponding reference lines (each subplot's reference line corresponds to the fitting line for  $\mu_A = \mu_B$  data at each concentration and particle size ratio). This observation confirms the robustness of the macroscopic friction effects and highlights how the coefficient scaling, due to particle size ratios, reflects the structural origins of these effects.

#### IV. CONCLUSION

In conclusion, our MD simulations revealed that the overall frictional strength in granular systems, represented by an

effective friction coefficient ( $\mu_e$ ), follows a power-law relationship with the individual friction coefficients. This finding enabled us to develop predictive models that can accurately describe the packing structure of binary mixtures of particles, considering variations in composition, size ratio, and preparation protocol. These models offer valuable insights into the behavior of complex granular systems, enhancing our understanding of the influence of friction on packing structure, and have implications for the dynamics of realistic granular systems. Further experimental validation of the models proposed in this work and extending them to compositionally more complex systems are valuable.

#### DATA AVAILABILITY

The data that support the findings of this study are available from the corresponding authors upon reasonable request.

- 
- [1] S. Torquato and F. H. Stillinger, Jammed hard-particle packings: From Kepler to Bernal and beyond, *Rev. Mod. Phys.* **82**, 2633 (2010).
- [2] L. P. Kadanoff, Built upon sand: Theoretical ideas inspired by granular flows, *Rev. Mod. Phys.* **71**, 435 (1999).
- [3] H. M. Jaeger, S. R. Nagel, and R. P. Behringer, Granular solids, liquids, and gases, *Rev. Mod. Phys.* **68**, 1259 (1996).
- [4] P. G. de Gennes, Granular matter: A tentative view, *Rev. Mod. Phys.* **71**, S374 (1999).
- [5] A. Baule, F. Morone, H. J. Herrmann, and H. A. Makse, Edwards statistical mechanics for jammed granular matter, *Rev. Mod. Phys.* **90**, 015006 (2018).
- [6] B. Kou *et al.*, Granular materials flow like complex fluids, *Nature (London)* **551**, 360 (2017).
- [7] A. J. Liu and S. R. Nagel, The jamming transition and the marginally jammed solid, *Annu. Rev. Condens. Matter Phys.* **1**, 347 (2010).
- [8] S. R. Nagel, Experimental soft-matter science, *Rev. Mod. Phys.* **89**, 025002 (2017).
- [9] N. Vandewalle, G. Lumay, O. Gerasimov, and F. Ludewig, The influence of grain shape, friction and cohesion on granular compaction dynamics, *Eur. Phys. J. E* **22**, 241 (2007).
- [10] A. P. Santos, D. S. Bolintineanu, G. S. Grest, J. B. Lechman, S. J. Plimpton, I. Srivastava, and L. E. Silbert, Granular packings with sliding, rolling, and twisting friction, *Phys. Rev. E* **102**, 032903 (2020).
- [11] L. E. Silbert, G. S. Grest, and J. W. Landry, Statistics of the contact network in frictional and frictionless granular packings, *Phys. Rev. E* **66**, 061303 (2002).
- [12] H. A. Makse, David. L. Johnson, and Lawrence. M. Schwartz, Packing of compressible granular materials, *Phys. Rev. Lett.* **84**, 4160 (2000).
- [13] M. Jerkins, M. Schroter, H. L. Swinney, T. J. Senden, M. Saadatfar, and T. Aste, Onset of mechanical stability in random packings of frictional spheres, *Phys. Rev. Lett.* **101**, 018301 (2008).
- [14] L. E. Silbert, Jamming of frictional spheres and random loose packing, *Soft Matter* **6**, 2918 (2010).
- [15] X. L. Sun, W. Kob, R. Blumenfeld, H. Tong, Y. J. Wang, and J. Zhang, Friction-controlled entropy-stability competition in granular systems, *Phys. Rev. Lett.* **125**, 268005 (2020).
- [16] J. D. Bernal and J. Mason, Packing of spheres: Co-ordination of randomly packed spheres, *Nature (London)* **188**, 910 (1960).
- [17] D. W. Cooper, Random-sequential-packing simulations in three dimensions for spheres, *Phys. Rev. A* **38**, 522 (1988).
- [18] J. L. Finney, Random packings and the structure of simple liquids. I. The geometry of random close packing, *Proc. R. Soc. London A* **319**, 479 (1970).
- [19] M. van Hecke, Jamming of soft particles: Geometry, mechanics, scaling and isostaticity, *J. Phys-Condens. Mat.* **22**, 033101 (2010).
- [20] K. Shundyak, M. van Hecke, and W. van Saarloos, Force mobilization and generalized isostaticity in jammed packings of frictional grains, *Phys. Rev. E* **75**, 010301(R) (2007).
- [21] H. P. Zhang and H. A. Makse, Jamming transition in emulsions and granular materials, *Phys. Rev. E* **72**, 011301 (2005).
- [22] G. Y. Onoda and E. G. Liniger, Random loose packings of uniform sphere and the dilatancy onset, *Phys. Rev. Lett.* **64**, 2727 (1990).
- [23] Y. Xing, Y. Yuan, H. F. Yuan, S. Y. Zhang, Z. K. Zeng, X. Zheng, C. J. Xia, and Y. J. Wang, Origin of the critical state in sheared granular materials, *Nat. Phys.* **20**, 646 (2024).
- [24] Y. Yuan *et al.*, Experimental test of the Edwards volume ensemble for tapped granular packings, *Phys. Rev. Lett.* **127**, 018002 (2021).
- [25] A. Lemaitre, C. Mondal, I. Procaccia, S. Roy, Y. Q. Wang, and J. Zhang, Frictional granular matter: Protocol dependence of mechanical properties, *Phys. Rev. Lett.* **126**, 075501 (2021).
- [26] A. Lemaitre, C. Mondal, I. Procaccia, and S. Roy, Stress correlations in frictional granular media, *Phys. Rev. B* **103**, 054110 (2021).
- [27] F. J. Meng and K. Liu, Mechanical study on the effect of granular friction in a granular system under biaxial compression, *J. Korean Phys. Soc.* **72**, 1179 (2018).
- [28] Y. Yuan, Z. K. Zeng, Y. Xing, H. F. Yuan, S. Y. Zhang, W. Kob, and Y. J. Wang, From creep to flow: Granular materials under cyclic shear, *Nat. Commun.* **15**, 3866 (2024).

- [29] J. R. Royer and P. M. Chaikin, Precisely cyclic sand: Self-organization of periodically sheared frictional grains, *Proc. Natl. Acad. Sci. USA* **112**, 49 (2015).
- [30] I. Srivastava, L. E. Silbert, G. S. Grest, and J. B. Lechman, Flow-arrest transitions in frictional granular matter, *Phys. Rev. Lett.* **122**, 048003 (2019).
- [31] D. Berzi and J. T. Jenkins, Fluidity, anisotropy, and velocity correlations in frictionless, collisional grain flows, *Phys. Rev. Fluids* **3**, 094303 (2018).
- [32] C. Goldenberg and I. Goldhirsch, Friction enhances elasticity in granular solids, *Nature (London)* **435**, 188 (2005).
- [33] F. D. Cúñez, D. Patel, and R. C. Glade, How particle shape affects granular segregation in industrial and geophysical flows, *Proc. Natl. Acad. Sci. USA* **121**, e2307061121 (2024).
- [34] D. Dumont, P. Souillard, T. Salez, E. Raphaël, and P. Damman, Microscopic picture of erosion and sedimentation processes in dense granular flows, *Phys. Rev. Lett.* **125**, 208002 (2020).
- [35] J. D. Zhao, S. W. Zhao, and S. Luding, The role of particle shape in computational modelling of granular matter, *Nat. Rev. Phys.* **5**, 505 (2023).
- [36] D. J. Jerolmack and K. E. Daniels, Viewing Earth's surface as a soft-matter landscape, *Nat. Rev. Phys.* **1**, 716 (2019).
- [37] S. Plimpton, Fast parallel algorithms for short-range molecular dynamics, *J. Comput. Phys.* **117**, 1 (1995).
- [38] G. K. P. Barrios, R. M. de Carvalho, A. Kwade, and L. M. Tavares, Contact parameter estimation for DEM simulation of iron ore pellet handling, *Powder. Technol.* **248**, 84 (2013).
- [39] A. Di Renzo and F. P. Di Maio, An improved integral non-linear model for the contact of particles in distinct element simulations, *Chem. Eng. Sci.* **60**, 1303 (2005).
- [40] H. A. Makse, N. Gland, D. L. Johnson, and L. Schwartz, Granular packings: Nonlinear elasticity, sound propagation, and collective relaxation dynamics, *Phys. Rev. E* **70**, 061302 (2004).
- [41] I. Srivastava, S. A. Roberts, J. T. Clemmer, L. E. Silbert, J. B. Lechman, and G. S. Grest, Jamming of bidisperse frictional spheres, *Phys. Rev. Res.* **3**, L032042 (2021).
- [42] K. Kamrin, K. M. Hill, D. I. Goldman, and J. E. Andrade, Advances in modeling dense granular media, *Annu. Rev. Fluid Mech.* **56**, 215 (2024).
- [43] H. F. Yuan, Z. Zhang, W. Kob, and Y. J. Wang, Connecting packing efficiency of binary hard sphere systems to their intermediate range structure, *Phys. Rev. Lett.* **127**, 278001 (2021).